A Universal Model Predictive Control Strategy for Dual Inverters Fed OW-PMSM Drives

Yancheng Chen, *Student Member, IEEE*, Xueqing Wang, *Member, IEEE*, Xin Meng, *Member, IEEE*, Mingzhi He, *Member, IEEE*, Dianxun Xiao, *Member, IEEE*, and Zheng Wang, *Senior Member, IEEE*

***Abstract*—This article proposed a universal model predictive control (MPC) strategy for dual inverters fed open-winding permanent magnet synchronous motor drives where two isolated buses have arbitrary dc voltages. Diverse and unordered space vector distribution caused by different voltage ratios of dc buses that greatly increase the calculation burden for the conventional MPC algorithm is analyzed in detail. Based on this, a novel MPC strategy that is universally applicable to any voltage ratio is put forward, which could decrease the number of candidate vectors from 49 to less than 15 in every cycle. Although the computational burden is reduced, the output power quality is unaffected owing to the effective simplification of the vectors. Besides, an optimized switching algorithm is designed to adapt to the situation when the voltage ratio changes during the operation state. The experimental results are presented to verify the effectiveness of the proposed method.**

***Index Terms*—Dual inverters, model predictive control (MPC), open-winding permanent magnet synchronous motor (OW-PMSM), space voltage vectors, unfixed dc-link voltage ratios.**

I. Introduction

THE open-winding permanent magnet synchronous motor (OW-PMSM) can be seen as a kind of special three-phase motor that is formed by opening the neutral point of conventional start-connected motors, and equipping the motor with dual inverters on both sides [1], [2]. By combining OW configuration and dual two-level inverters, OW-PMSM drives have the benefits of multilevel characteristics, high-voltage utilization, flexible control, and good fault-tolerant capability [3], [4], [5], [6], [7], [8]. The multilevel characteristics can help to reduce the current harmonics and electromagnetic interference [9], [10], [11]. All these merits contribute to the rising attention drawn by OW-PMSM drives.

According to the different dc-link power supply modes of the dual inverters, OW-PMSM drives could be divided into two categories as below: the common bus mode and the independent bus mode [5]. OW-PMSM drives with common dc buses have relatively low unit costs and high-power density [6]. However, dual inverters sharing a common bus could lead to zero-sequence currents and increase the loss. So extra control schemes are required to restrain zero-sequence currents in this topology [7]. By comparison, the OW-PMSM with independent dc buses could avoid this trouble because the zero-sequence current path is blocked [8]. To reduce the cost of independent power supplies, a floating capacitor instead of a voltage source could be connected to one of the dc buses, which could provide voltage support and reactive power in certain situations [12]. However, the dc bus supplied by a capacitor is unable to continuously output active power and specialized control is needed to balance capacitor voltage, which limits its application to some extent [13]. By comparison, OW-PMSM drives with two independent power sources could achieve a more stable energy supply and a higher voltage utilization. Additionally, the voltages of the dc buses supplied by independent voltage sources are also easier to maintain than the capacitor-fed buses.

When the two dc links are not connected directly, different voltage ratios of the two sides could be adopted to meet diverse specific requirements. For example, when the voltage ratio of dc buses is set to 1:1, the inverters could generate a three-level output voltage waveform [14]. Similarly, the inverters could also attain an equivalent four-level effect when the voltage ratio is configured as 2:1 [15]. It could be generalized to the situation of the ratio K:1, i.e., the ratio of dc buses is not restricted. In this way, the inverters could generate diverse vector distributions, and more control degrees of freedom could be gained [16]. In addition to the special voltage ratios mentioned above, the multilevel effect could also be obtained with nonspecial voltage ratios, which also contribute to lower output total harmonic distortion (THD) [17], [18]. In [17], different voltage ratios are discussed and compared from the aspects of voltage utilization and power quality. In [18], a unified modulation method with novel region division and vector synthesis is proposed for the OW-PMSM fed by dual sources with arbitrary voltage ratios. In [16], a lookup table strategy is established for the direct torque control

Manuscript received 27 June 2022; revised 5 February 2023; accepted 16 March 2023. Date of publication 22 March 2023; date of current version 20 April 2023. This work was supported in part by the Science and Technology Projects of Sichuan Province under Grant 2019ZDZX0019, and in part by Natural Science Foundation of Sichuan Province under Grant 2022NSFSC1888. Recommended for publication by Associate Editor S. K. Panda. *(Corresponding authors: Xueqing Wang; Xin Meng.)*

Yancheng Chen, Xueqing Wang, Xin Meng, and Mingzhi He are with the College of Electrical Engineering, Sichuan University, Chengdu 610065, China (e-mail: cyrise@foxmail.com; xwang@scu.edu.cn; mengxin_pe@163.com; darmyhe@126.com).

Dianxun Xiao is with the Sustainable Energy and Environment Thrust, The Hong Kong University of Science and Technology (Guangzhou), Guangzhou 511458, China (e-mail: dianxunxiao@ust.hk).

Zheng Wang is with the School of Electrical Engineering, Southeast University, Nanjing 210096, China (e-mail: zwang@eee.hku.hk).

Color versions of one or more figures in this article are available at https://doi.org/10.1109/TPEL.2023.3260305.

Digital Object Identifier 10.1109/TPEL.2023.3260305

of OW-PMSM drives by analyzing the distribution patterns under different voltage ratios. In brief, the various voltage ratios could produce different voltage vector effects, which greatly improve the flexibility and the power quality of the OW-PMSM systems.

Finite control set–model predictive control (FCS–MPC) of motor drives, which selects the optimal vector through the cost function, has the merits of good dynamic performance, multiobjective control, and low switching frequency [19], [20], [21]. However, under the circumstance of the K:1 ratio, the multivector distribution is complicated and irregular, and this brings an excessive computational burden on calculating all the possibilities [21]. So it is necessary to simplify the candidate vectors according to the voltage ratios. In [22], a simplified MPC strategy is proposed for an equivalent three-level OW-PMSM system to reduce the calculation burden by picking the optimal vector with twice sector judgments. But this method relies on sector division and does not apply to the case of arbitrary voltage ratios. A predictive torque control that reduces the redundant computation in the traversal procedure is introduced in [23], the control strategy of which uses the location of the stator flux vector to reduce candidate vectors into half. But traversing all 20 candidate vectors is still a time-consuming process. In [24], a four-level MPC scheme is proposed for the OW induction motor drive powered by a voltage source and a floating capacitor. A cascaded two-step vector selection method is designed to determine the output voltage vector. But when the voltage ratio is not fixed to 2:1, the first step of the vector selection process may cause errors.

In this article, a universal MPC strategy is proposed for OW-PMSM drives supplied by isolated dc buses with arbitrary voltage ratios. First, the vector distributions under different voltage ratios are constructed into five cases and their impacts on the power quality are analyzed in detail. Then, an approach of vector state classification is developed according to the output vector in the last control cycle to obtain the candidate vectors under different voltage ratios. Finally, the optimal vector will be obtained by traversing the candidate vectors with the cost function. The major contributions of this article can be summarized as follows:

1) The proposed MPC strategy is universally applicable for OW-PMSM drives with any voltage ratios of dc buses.
2) The candidate vectors can be simplified from 49 to less than 15 under different voltage ratios, which greatly reduces the calculation burden.
3) The proposed MPC strategy can include all the adjacent vectors into the selection scope to find the optimal vector, which guarantees good control accuracy and power quality.

The rest of this article is as follows. In Section II, the configuration of the OW-PMSM system with an unfixed voltage ratio is introduced and modeled. Section III analyzes the principle of traditional MPC. Then, a universal MPC strategy that is applicable to variable voltage ratios is proposed in Section IV. In Section V, experimental results are given to prove the effectiveness of the proposed method. Finally, this article is concluded in Section VI.

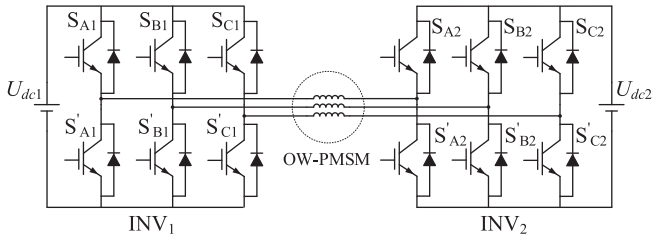

Fig. 1. OW-PMSM drive with independent DC buses.

II. Modeling of OW-PMSM Drives

Fig. 1 shows the topology of OW-PMSM drives with two independent dc buses. The voltage ratio of the two voltage sources is flexible. The inverter with the higher dc voltage is defined as the master inverter, and the other one is identified as the slave inverter. Accordingly, their dc-link voltages are named as U_{dcm} and U_{dcs}, with the relation of $U_{\text{dcm}} \geq U_{\text{dcs}}$.

A. Modeling of the OW-PMSM

The voltage equations OW-PMSM in the three-phase static reference frame can be given as

$$\begin{bmatrix} u_A \\ u_B \\ u_C \end{bmatrix} = \frac{d}{dt} \begin{bmatrix} \psi_A \\ \psi_B \\ \psi_C \end{bmatrix} + \begin{bmatrix} R_s & 0 & 0 \\ 0 & R_s & 0 \\ 0 & 0 & R_s \end{bmatrix} \begin{bmatrix} i_A \\ i_B \\ i_C \end{bmatrix} \tag{1}$$

where $u_{A,B,C}$, $\psi_{A,B,C}$, and $i_{A,B,C}$ stand for phase-voltages, the stator magnet flux linkages, and phase-currents, respectively. R_s denotes the resistance of motor windings.

Since the two dc buses are not linked together, the zero-sequence current does not exist and the zero-sequence dimension can be omitted. Through the Park transformation, (1) could be expressed as follows in the dq-axis reference frame:

$$\begin{bmatrix} u_d \\ u_q \end{bmatrix} = R_s \begin{bmatrix} i_d \\ i_q \end{bmatrix} + \frac{d}{dt} \begin{bmatrix} \psi_d \\ \psi_q \end{bmatrix} + \omega_e \begin{bmatrix} -\psi_q \\ \psi_d \end{bmatrix} \tag{2}$$

where $u_{d,q}$, $\psi_{d,q}$, and $i_{d,q}$ denote the dq-axis voltages, magnet flux linkages, and currents, respectively. ω_e represents the electrical angular speed.

The relationships between fluxes and currents in the dq-axis reference frame can be expressed as

$$\begin{bmatrix} \psi_d \\ \psi_q \end{bmatrix} = \begin{bmatrix} L_d & 0 \\ 0 & L_q \end{bmatrix} \begin{bmatrix} i_d \\ i_q \end{bmatrix} + \begin{bmatrix} \psi_f \\ 0 \end{bmatrix} \tag{3}$$

where $\psi_{d,q}$ and ψ_f stand for magnet flux linkages of the dq-axis and the permanent magnet flux linkage, respectively. $L_{d,q}$ is the stator inductance in the dq-axis.

By substituting (3) into (2), the voltages in the dq-axis reference frame can be further expressed as

$$\begin{bmatrix} u_d \\ u_q \end{bmatrix} = R_s \begin{bmatrix} i_d \\ i_q \end{bmatrix} + \frac{d}{dt} \begin{bmatrix} L_d & 0 \\ 0 & L_q \end{bmatrix} \begin{bmatrix} i_d \\ i_q \end{bmatrix} + \omega_e \begin{bmatrix} -L_q i_q \\ L_d i_d + \psi_f \end{bmatrix}. \tag{4}$$

The electromagnetic torque could be represented with the dq-axis currents as

$$T_e = \frac{3}{2}N_p[\psi_f i_q + (L_d - L_q)i_d i_q] \tag{5}$$

where N_p is the number of pole pairs.

B. Modeling of the Inverters

For the OW-PMSM drives with independent dc buses, the phase voltages are determined by dual inverters' switching states and the dc-link voltages from both sides. The switching states of Phase-A, Phase-B, and Phase-C from the master inverter or the slave inverter are defined as $S_{A,B,C/m,s}$ (1 for high level and 0 for low level). By using different voltage vectors from $V1(100)$–$V7(111)$, the phase voltages of the OW-PMSM drives can be expressed with the switching states of the master inverter and the slave inverter as

$$\begin{bmatrix} u_A \\ u_B \\ u_C \end{bmatrix} = \begin{bmatrix} u_{Am} - u_{As} \\ u_{Bm} - u_{Bs} \\ u_{Cm} - u_{Cs} \end{bmatrix} = \frac{1}{3}\begin{bmatrix} 2 & -1 & -1 \\ -1 & 2 & -1 \\ -1 & -1 & 2 \end{bmatrix} \times \left(U_{\text{dcm}} \begin{bmatrix} S_{Am} \\ S_{Bm} \\ S_{Cm} \end{bmatrix} - U_{\text{dcs}} \begin{bmatrix} S_{As} \\ S_{Bs} \\ S_{Cs} \end{bmatrix} \right). \tag{6}$$

III. Principle of Model Predictive Control

A. Discrete Predictive Equations

Since FCS–MPC is fulfilled by selecting the optimal one from the finite candidates, the model of OW-PMSM discussed in Section II needs to be transformed into the discrete domain. The first-order Eula method in the following equation could be employed to discretize the OW-PMSM system model, which can obtain satisfactory results and guarantee fast calculation speed

$$\frac{dx}{dt} = \frac{x^{k+1} - x^k}{T_s}. \tag{7}$$

By discretizing (4) with the Eula method in (7), the dq-axis predicted currents in the discrete domain can be obtained as

$$\begin{bmatrix} i_d^{k+1} \\ i_q^{k+1} \end{bmatrix} = \begin{bmatrix} i_d^k \\ i_q^k \end{bmatrix} + \begin{bmatrix} \left(u_d^k - R_s i_d^k + \omega_e L_q i_q^k\right)\frac{T_s}{L_d} \\ \left(u_q^k - R_s i_q^k - \omega_e L_d i_d^k\right)\frac{T_s}{L_q} \end{bmatrix} - \begin{bmatrix} 0 \\ \omega_e \psi_f \frac{T_s}{L_q} \end{bmatrix} \tag{8}$$

where $i_{d,q}^{k+1}$ stand for the dq-axis currents of the $(k+1)$th cycle, and $u_{d,q}^k$, $i_{d,q}^k$ denote the dq-axis sampled voltages and currents in the present switching period, respectively.

B. Prediction Calculation

When MPC is applied to practical systems, it costs time for MCUs to update the optimal voltage vector, causing the vector calculation results could not be applied in the present control period immediately. Therefore, one-beat delay compensation should be exerted on the system to eliminate errors.

For ease of elaboration, the output effect on the OW-PMSM could be represented by V_s^k, namely the vector difference between the master inverter and the slave inverter

$$V_s^k = V_{\text{INV}m}^k - V_{\text{INV}s}^k. \tag{9}$$

With the optimal output voltage vector V_s^k, which is obtained from the last control period and applied in the present cycle, the system state $i_{d,q}^{k+1}$ and $u_{d,q}^{k+1}$ could be calculated through the delay compensation with the predictive model. As the compensated currents of the dq-axis $i_{d,q}^{k+1}$ are obtained through (8), the predicted currents of the candidate vectors $i_{d,q}^{k+2}$ could be calculated by a prediction calculation

$$\begin{bmatrix} i_d^{k+2} \\ i_q^{k+2} \end{bmatrix} = \begin{bmatrix} i_d^{k+1} \\ i_q^{k+1} \end{bmatrix} + \begin{bmatrix} \left(u_d^{k+1} - R_s i_d^{k+1} + \omega_e L_q i_q^{k+1}\right)\frac{T_s}{L_d} \\ \left(u_q^{k+1} - R_s i_q^{k+1} - \omega_e L_d i_d^{k+1}\right)\frac{T_s}{L_q} \end{bmatrix} - \begin{bmatrix} 0 \\ \omega_e \psi_f \frac{T_s}{L_q} \end{bmatrix} \tag{10}$$

where $i_{d,q}^{k+2}$ denotes the reference currents of the dq-axis.

The accuracy of current predictions in (10) can be further improved by considering the predictions of rotor speed and rotor positions [25]. Considering that this article focuses on the analysis and optimization selection of candidate vectors for the OW-PMSM drive with different voltage ratios, the predictions of rotor speed and rotor position are not studied in this article.

C. Cost Function

In order to find the optimal one from the candidate vectors, a cost function could be designed as (11). With the cost function F, the control objectives of the d-axis and q-axis in two dimensions can be realized in one equation

$$F = \left|i_d^{\text{ref}} - i_d^{k+2}\right| + \left|i_q^{\text{ref}} - i_q^{k+2}\right| \tag{11}$$

where $i_{d,q}^{\text{ref}}$ stand for the reference currents of the dq-axis.

Afterward, all the candidate space vectors are traversed, and the optimal one could be determined through the cost function.

IV. Proposed MPC Strategy

The dual inverters with unfixed dc-link voltage could generate 49 space voltage vectors, considering that the inverter on each side could produce 7 different vector effects. Thus, it is necessary to simplify the vector selection strategy of MPC, otherwise, the heavy computational burden is not acceptable for most controllers.

The block diagram of the proposed MPC strategy with a simplified selection scheme of candidate vectors is shown in Fig. 2. With the output voltage vector applied to the present control cycle, the candidate vectors for the cost function could be determined by the state identification procedure. The dq-axis currents of the present period can also be computed by using V_s^k to compensate for the time delay of one cycle. Finally, the optimal vector V_s^{k+1} can be obtained by comparing the candidate vectors through the cost function.

Since the output voltage vector can make a fast change of the motor currents in one control cycle, using the MPC in the internal

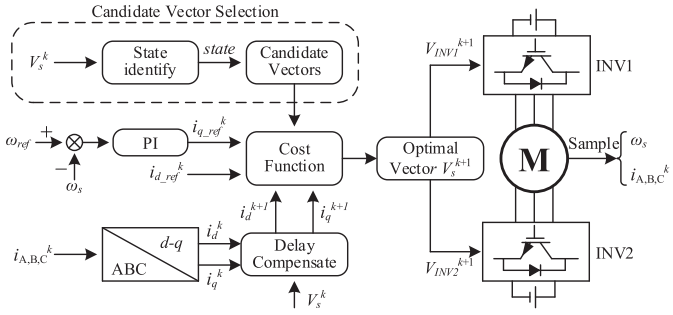

Fig. 2. Block diagram of proposed MPC strategy.

current loop can significantly improve the current response performance of the OW-PMSM drive. Due to the impact of the moment of inertia in the motor, the mechanical response speed is much slower than the electrical response speed. Considering the widespread application of the vector control, using a PI controller in the external speed loop in Fig. 2 could meet the requirements of dynamic stability in most drive applications and provide excellent steady-state control precision.

A. Space Vectors of Unfixed DC Voltage Ratios

With the constraint of $U_{\rm dcm} \geq U_{\rm dcs}$, the situations of space vector distribution can be concluded into two equal intervals according to the relationships between $U_{\rm dcs}$ and $U_{\rm dcm}/2$, i.e., $U_{\rm dcs} \in (0, U_{\rm dcm}/2)$ and $U_{\rm dcs} \in (U_{\rm dcm}/2, U_{\rm dcm})$. Additionally, when $U_{\rm dcs}$ is equal to 0, $U_{\rm dcm}/2$, and $U_{\rm dcm}$, the dual inverters could generate an equivalent effect of two-level, three-level, and four-level, respectively. Thus, five cases are supposed to be considered to cover all different voltage ratios of dual inverters.

Fig. 3 shows different cases of voltage vector distributions from the single inverter and dual inverters, in which each dot represents a voltage vector. For better presentation, the vectors with the same effect are placed in an adjacent way rather than an overlapping way. Two hexagons are marked with green in the center and yellow in the upper-right area to, respectively, distinguish the effects of the master inverter and slave inverter. From Case-1 to Case-5, the voltage ratio changes from 1:0 to 1:1 with the voltage $U_{\rm dcs}$ increases, among which the effect of Case-1 is actually equivalent to that of the star-connected PMSM. It can be seen that the voltage vector distributions are not fixed under different voltage ratios, but the changeable vectors are always located in specific straight lines.

B. Vector Distribution and Power Quality

According to the space vector diagrams in Fig. 3, the distance between the voltage vectors in the diagram will change with the voltage ratio. When the distance between the output vector and the ideal reference vector increases, the error between the output voltage and the ideal voltage will become larger, and the output power quality of the dual inverters will be degraded. Since the MPC method could select the vector with the smallest distance from the ideal reference vector as output, the maximum voltage errors under different voltage ratios can be obtained according

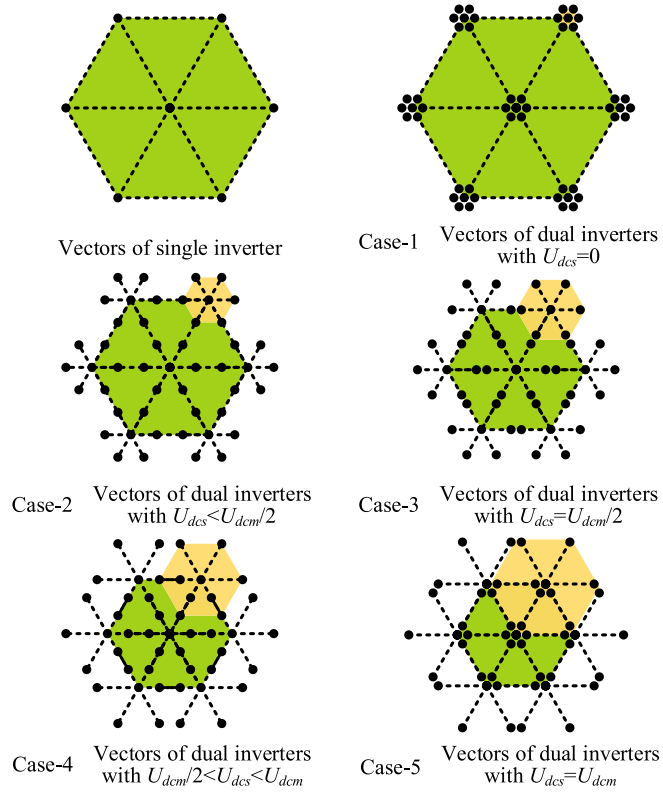

Fig. 3. Space vector diagram of different voltage ratios.

to the distance between the output vector and the ideal reference vector, which could reflect the worst situation of output power quality under different voltage ratios.

In Case-1, the space vector diagram presents the typical two-level characteristics. In this case, the maximum voltage error between the ideal reference vector and the output vector will reach the maximum value when the ideal reference vector is located in the center of the subsector triangle. As for Case-2, namely $U_{\rm dcs} < U_{\rm dcm}/2$, the slave inverter side comes into effect, and the maximum voltage error will decrease with the increase of $U_{\rm dcs}$. When the voltage ratio is 2:1 in Case-3, the maximum voltage error is still in the process of decreasing. In Case-4, the maximum voltage error starts to increase with $U_{\rm dcs}$. In the situation of Case-5, namely $U_{\rm dcs} = U_{\rm dcm}$, the maximum voltage error will reach the other peak beside Case-1. Based on the above analysis, the relationship between the maximum voltage vector error $U_{\rm max}$ and two dc-link voltages $U_{\rm dcm}$ and $U_{\rm dcs}$ could be uniformly expressed as follows by using the Pythagorean theorem in a subsector triangle

$$U_{\rm max}^2 = \left(\frac{\sqrt{3}}{9}U_{\rm dcm}\right)^2 + \left(\frac{1}{3}U_{\rm dcm} - \frac{2}{3}U_{\rm dcs}\right)^2. \tag{12}$$

According to (12), the maximum voltage error $U_{\rm max}$ can be solved and simplified as

$$U_{\rm max} = \frac{2\sqrt{3}}{9}\sqrt{U_{\rm dcm}^2 - 3U_{\rm dcm}U_{\rm dcs} + 3U_{\rm dcs}^2}. \tag{13}$$

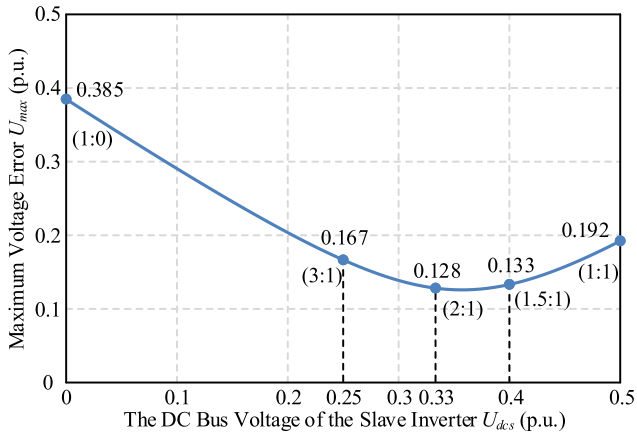

Fig. 4. Relationship between $U_{\max}$ and U_{dcs}.

In order to establish reasonable evaluation and comparison, the voltage sum of two dc-links $U_{\sum}$ is set to be constant. In this way, the maximum voltage error $U_{\max}$ can be expressed with U_{dcs} and $U_{\sum}$ as

$$U_{\max} = \frac{2\sqrt{3}}{9}\sqrt{U_{\sum}^2 - 5U_{\mathrm{dcs}}U_{\sum} + 7U_{\mathrm{dcs}}^2}. \tag{14}$$

According to (14), the function curve of the relationship between the maximum voltage error $U_{\max}$ and the slave dc-link voltage U_{dcs} can be plotted in the form of per unit with respect to $U_{\sum}$, namely $U_{\sum} = 1$, as shown in Fig. 4. It can be seen from Fig. 4 that the maximum vector errors are relatively large at the voltage ratios of 1:0 and 1:1, while the voltage vector errors are relatively small at the voltage ratios of 3:1, 2:1, and 1.5:1. Therefore, of the inverters also follows a similar rule, that is, the THD decreases first and then increases. In general, the worst situation of current harmonics in OW-PMSM drive is positively correlated with the maximum voltage error $U_{\max}$.

The applicable condition of the above formulas and analysis is $U_{\mathrm{dcm}} \geq U_{\mathrm{dcs}}$, as is mentioned in Section II. The case of $U_{\mathrm{dcm}} < U_{\mathrm{dcs}}$ can also be resolved by reassigning the master and slave inverters, which will be introduced in Section IV-E.

Low switching frequency is the inherent characteristic of the MPC method since only a single voltage vector is selected for output in every control cycle, which will increase current harmonics, but can also reduce the switching loss of the inverter. It has been widely recognized that current harmonics will cause an extra loss in motor drives [26]. In this article, the multilevel effect of the OW-PMSM drive with an arbitrary voltage ratio is fully utilized in the proposed MPC strategy to reduce the current harmonics with low switching frequency. The switching frequency in the proposed MPC strategy can be further optimized to reach a balance between inverter efficiency and motor efficiency according to different practical drive applications.

C. Candidate Vector Classification

When the motor is running, the reference voltage vector changes in a continuous way in the vector diagram. Therefore, as the output vector of the previous cycle is already known, the optimal vector of the present step should be close to it. Thus, only the vectors adjacent to the optimal vector in the last control cycle should be considered as the candidate vectors [27]. Because the distribution of the vector diagram is uncertain, all the possibilities need to be considered.

As Table I shows, the distribution of the candidate vectors could be classified into three states on the basis of the output vector of the previous cycle which is marked with blue dots in the vector diagrams. In each state, the candidate vectors that are adjacent to the last output vector are represented by red dots. Five cases with different voltage ratios are all included in every state. The symbol V, V' is used to represent the vectors generated by dual inverters, in which V denotes the vector from the master inverter and V' stands for the vector generated by the slave inverter. The effects of space vectors generated by $V0(000)$ and $V7(111)$ are the same, so $V7(111)$ could be used to uniformly represent the zero vector in this article. Thus, the value range of VV' is $V, V' \in [1, 7]$. The three states of the space vector classification are elaborated as follows:

1) *State-1:* When the output vector applied to the present control cycle is zero vector ($V_s^k = 77$), it is unable to determine which of the voltage vectors are closer to the zero vector, due to the unfixed voltage ratio. Thus, all the 12 voltage vectors in the vicinity of the zero vector need to be considered. One condition is that the two vector components could be in an opposite direction, namely $V_s^k = 11,22 \ldots 66$. And the other condition is that $V_{\mathrm{INV}m}^k$ is the zero vector and $V_{\mathrm{INV}s}^k$ is an arbitrary nonzero vector, namely $V_s^k = 71,72 \ldots 77$. Thus, in this state, a total of 13 vectors are selected as candidate vectors, including 77 itself.
2) *State-2:* When the previous output vector V_s^k is in the same direction as one of the diagonals in the master inverter hexagon, for example, $V_s^k = 11,74,17$, or 14, there are 10 candidate voltage vectors adjacent to the diagonal direction. Besides, additional five vectors that are in collineation with V_s^k should also be considered. Hence, 15 vectors in all are selected as candidate vectors aggregately under State-2.
3) *State-3:* If the voltage vector V_s^k is situated between two half-diagonals of the central hexagon, $V_s^k = 16,15,23,24 \ldots$ for instance, as is marked red in Table I, each diagonal leading or lagging behind V_s^k contains four vectors. Besides, their common point vector 77 should also be selected. Consequently, this state requires 13 candidate vectors altogether.

Through the proposed candidate vector classification method above, less than 15 candidate vectors instead of 49 candidate vectors will be selected for evaluation in the following process, which could greatly reduce the computational burden of MPC.

D. Optimal Vector Selection

Fig. 5 shows the flowchart of the proposed MPC strategy. First, the basic variables are obtained to support the MPC strategy. After compensating for the delay problem with (8), the key procedure of the proposed MPC strategy, namely candidate vector

TABLE I
VECTOR STATE CLASSIFICATION OF DIFFERENT VOLTAGE RATIOS

State-1	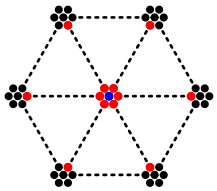	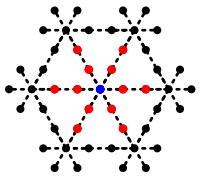	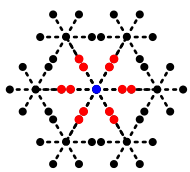	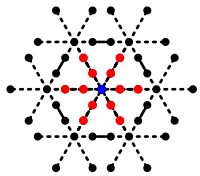	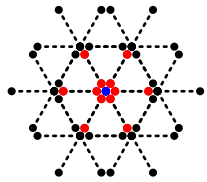
State-2	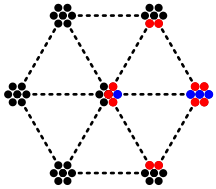	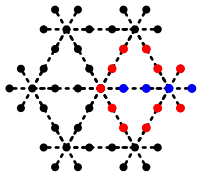	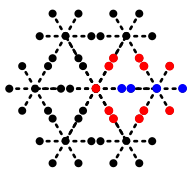	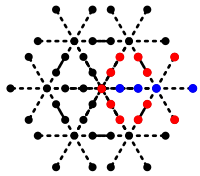	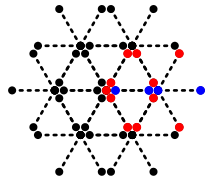
State-3	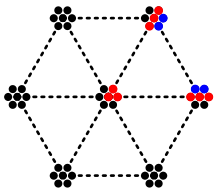	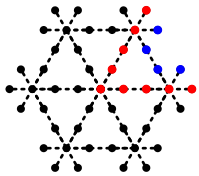	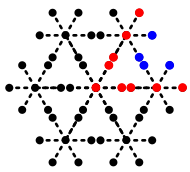	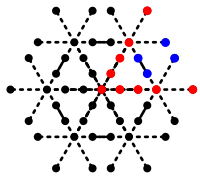	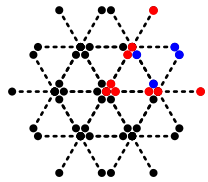
	U_{dcs}=0	U_{dcs}<U_{dcm}/2	U_{dcs}=U_{dcm}/2	U_{dcm}/2<U_{dcs}<U_{dcm}	U_{dcs}=U_{dcm}

selection, is conducted. By using the vector state classification in Table I, the vector state can be identified according to the output vector in the last cycle. Then, 13 or 15 candidate vectors will be selected based on the presently identified vector state and the output vector in the last cycle. After traversing all the candidate vectors through the current prediction in (10) and cost function calculation in (11), the optimal vector V_s^{k+1} will be finally determined.

E. Assignment of the Master and Slave Inverter

Since the master–slave relationship of the dual inverters is not fixed but determined by the relation of their dc-link voltages, it is necessary to design the switching algorithm of the master inverter and slave inverter.

At the beginning of every control cycle, a voltage judgment is performed. The inverter with a higher dc-link voltage is defined as the master inverter, and the other one is designated as the slave inverter. So when analyzing the space vector distribution, vectors from the master inverter that have larger vector distribution always constitute the central hexagon in the vector diagram. Thus, in the case of $U_{\mathrm{dc1}} \geq U_{\mathrm{dc2}}$, INV1 acts as the master inverter, and the vectors of the central hexagon in Fig. 3 are composed of vectors from INV1. As for the situation when $U_{\mathrm{dc2}} > U_{\mathrm{dc1}}$, the space vector hexagon of INV2 will be regarded as the central hexagon, and the slave inverter provides the vectors for the peripheral hexagons. After the optimal vector is picked out, the two components of the optimal vector are distributed to dual inverters based on the judgment of the master inverter and slave inverter.

When the master–slave relationship of the dual inverters changes in the process of running, the recorded output vectors of the master inverter and the slave inverter in the last cycle should be swapped with each other. Besides, since the directions of the phase voltages are related to the magnitude relationship between the dual inverters' voltages according to (6), the sampling phase currents should be reversed and the electrical angle of the motor should be adjusted by π. With the switching algorithm above, the proposed MPC strategy can be used for any voltage ratio.

TABLE II
EXPERIMENTAL PARAMETERS

Parameter	Symbol	Value
d-axis inductance	L_{d}	4 mH
q-axis inductance	L_{q}	4 mH
Stator resistance	R_s	0.9 Ω
PM flux linkage	ψ_f	0.375 Wb
Sampling frequency	f	5 kHz
DC-link capacitance	C	1000 μF

V. EXPERIMENTAL RESULTS

Experiments were conducted on the motor platform in Fig. 6 to demonstrate the validity of the proposed MPC strategy. Two separate dc sources supply power for the two dc buses of dual inverters. The microcontroller adopted in the experimental platform is DSP TMS320F28335 in the control board. The IGBTs are controlled by the pulsewidth modulation signal generated from the DSP through the IGBT drive. An external AD conversion chip AD7656 is used to ensure the accuracy of sampling signal processing for the current and voltage sensors. A load motor is coupled with the controlled OW-PMSM to provide load torque. Detailed experimental parameters are shown in Table II.

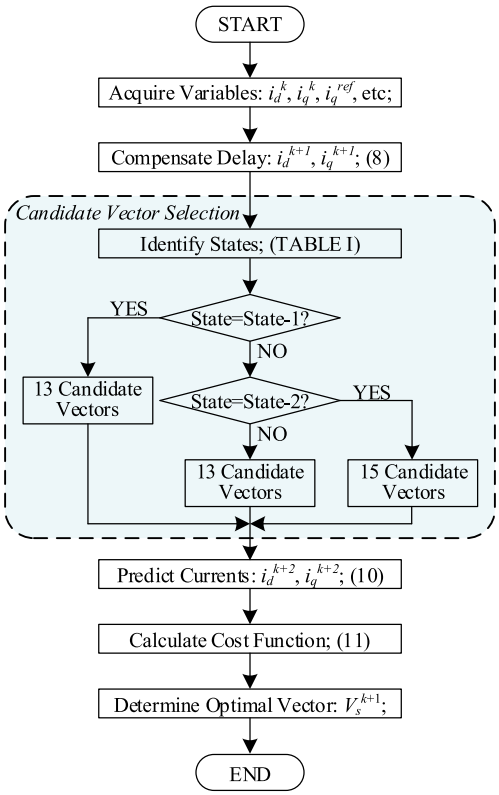

Fig. 5. Flowchart of the proposed MPC strategy.

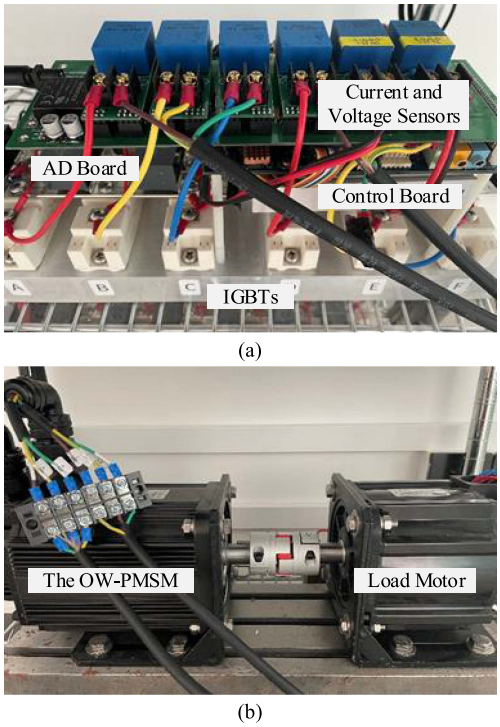

Fig. 6. Experimental platform.

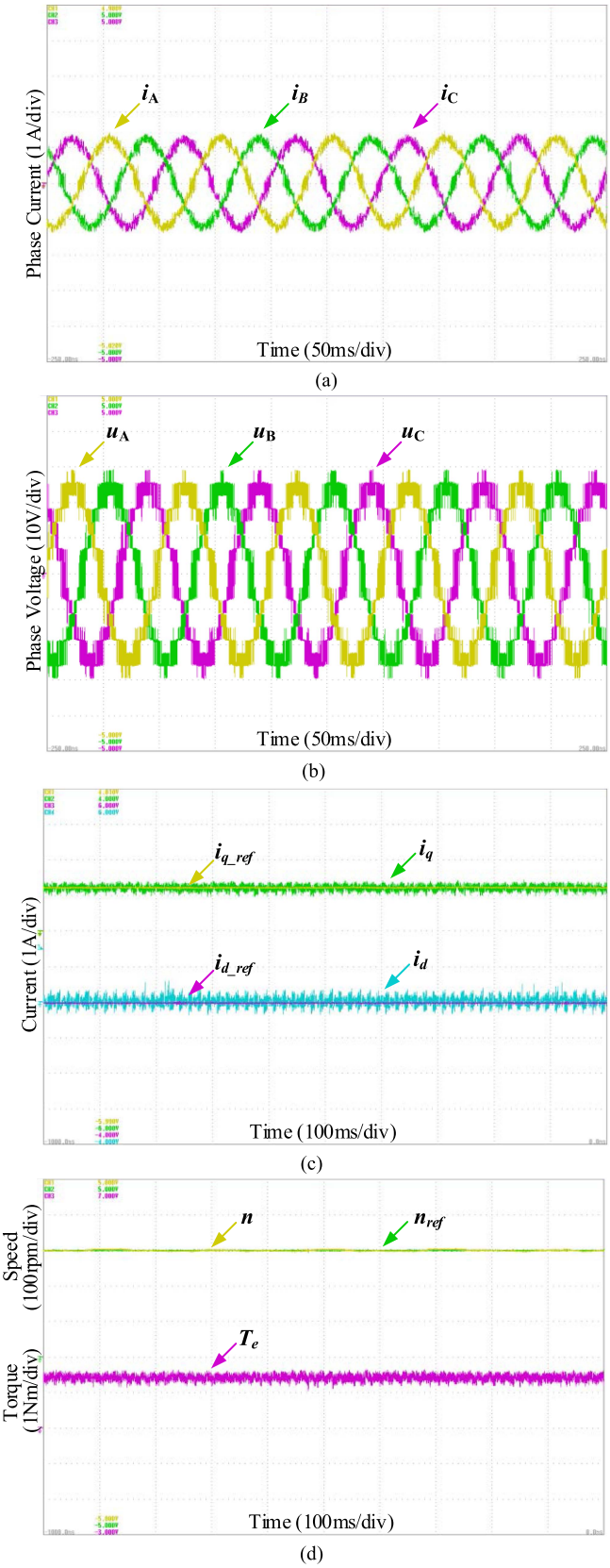

Fig. 7. Steady-state waveforms with the voltage ratio of 3:1. (a) Phase currents. (b) Phase voltages. (c) Currents of the *dq*-axis. (d) Motor speed and torque.

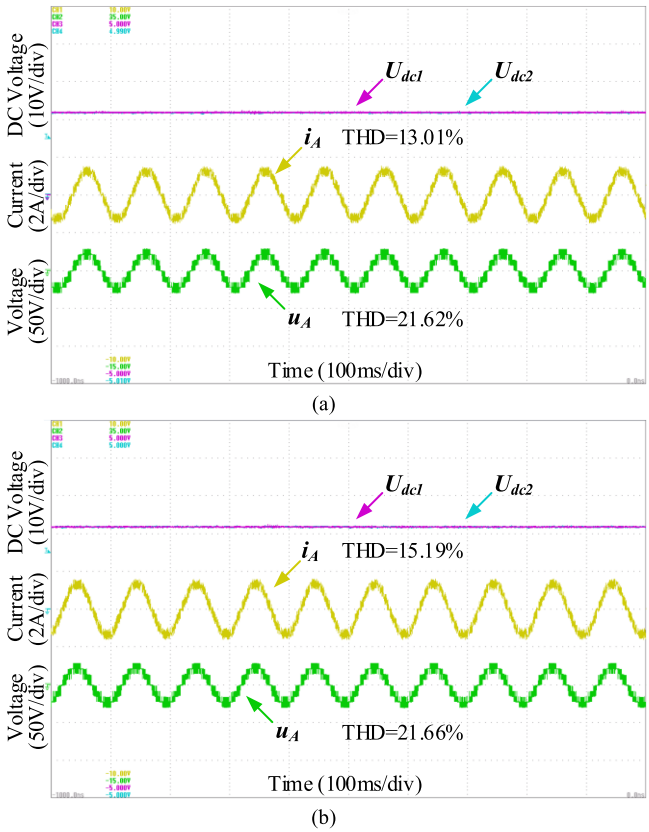

Fig. 8. Performance comparison under the voltage ratio of 1:1. (a) Proposed MPC strategy. (b) Conventional two-level MPC strategy.

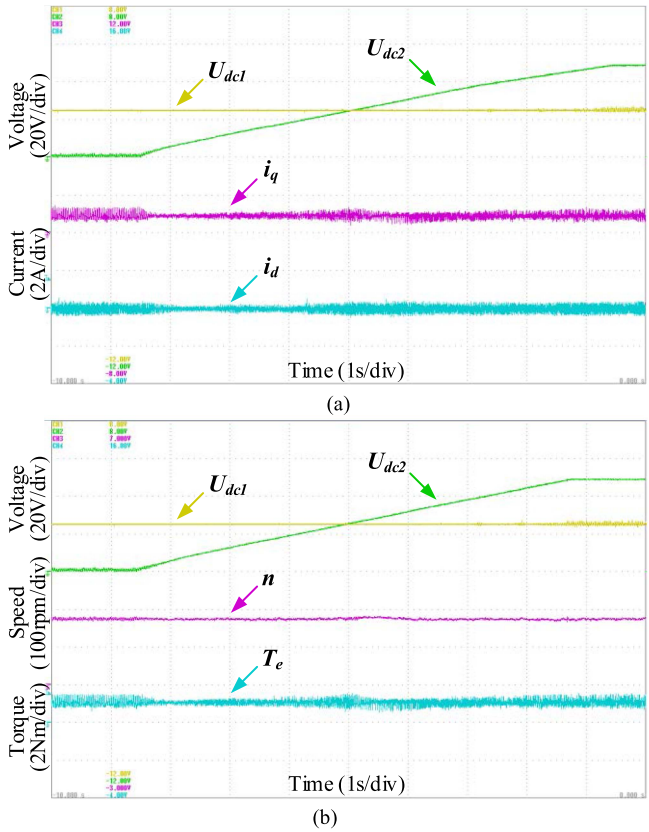

Fig. 9. Experimental waveforms under changing voltage ratio. (a) *dq*-axis currents. (b) Motor speed and output torque.

TABLE III
EXPERIMENTAL THD COMPARISON OF DIFFERENT MPC STRATEGIES

Voltage ratio	1:0	3:1	2:1	1.5:1	1:1
Strategy-I in [22]	46.14%	25.33%	18.14%	16.52%	16.36%
Strategy-II in [27]	44.40%	13.50%	11.05%	14.92%	21.11%
Proposed strategy	35.23%	11.85%	10.78%	13.01%	15.88%

Fig. 7 shows the steady-state performance of the proposed MPC strategy with the ratio of 3:1. It can be seen from Fig. 7(a) that the phase currents can present good sinusoidal waveforms, and the THD of phase currents is 11.85% in this case. Fig. 7(b) shows the multilevel phase voltages which guarantee high power quality. In Fig. 7(c) and (d), the *dq*-axis currents and the motor speed can track their corresponding references effectively, and the output torque is kept steady. Fig. 7 proves the effective multilevel output and current control of the proposed MPC for OW-PMSM drives.

Fig. 8 presents the comparison of phase currents and voltages between the proposed MPC strategy and the conventional MPC strategy which traverses all the voltage vectors under the ratio of 1:1. The THDs of Phase-A currents and voltages in the proposed strategy and the conventional strategy are 13.01%, 15.19% and 21.62%, 21.66%, respectively. Although many voltage vectors are excluded from the computational process in the proposed scheme, the output power quality is not affected. Besides, by comparison, the proposed MPC strategy can obviously reduce the computation burden and possess excellent flexibility in the ratio of two dc-link voltages.

To further illustrate the flexibility of the proposed MPC strategy in the aspect of voltage ratio, the output voltage of one power source is increased gradually from 0 to 50 V, while the other one keeps the constant voltage of 25 V, as is shown in Fig. 9. With the increase of the voltage in the changeable power source, the voltage ratio goes through 1:0, 3:1, 2:1, 1.5:1, 1:1, 1:1.5, 1:2, and other nonspecial values. It can be seen from Fig. 9 that the currents, torque, and speed can always remain stable with any voltage ratios. When the voltage ratio goes across 1:1, the dual inverters carry out the switching of the master inverter and the slave inverter. The smooth switching proves the effectiveness of the master–slave switching algorithm.

In Fig. 10(a) and (b), the voltage ratios are kept as 2:1 and 1:2, respectively, to show the impact of appointing INV1 or INV2 as the master inverter. Considering the change of the master–slave relationship in Fig. 10(a) and (b), the positive direction of the phase current sampling and the electrical angle are adjusted based on Section IV-E accordingly. Fig. 10(a) shows phase current and phase voltage when INV1 acts as the master inverter, while the circumstances that INV2 is selected as the master inverter is illustrated in Fig. 10(b). The THDs of Phase-A

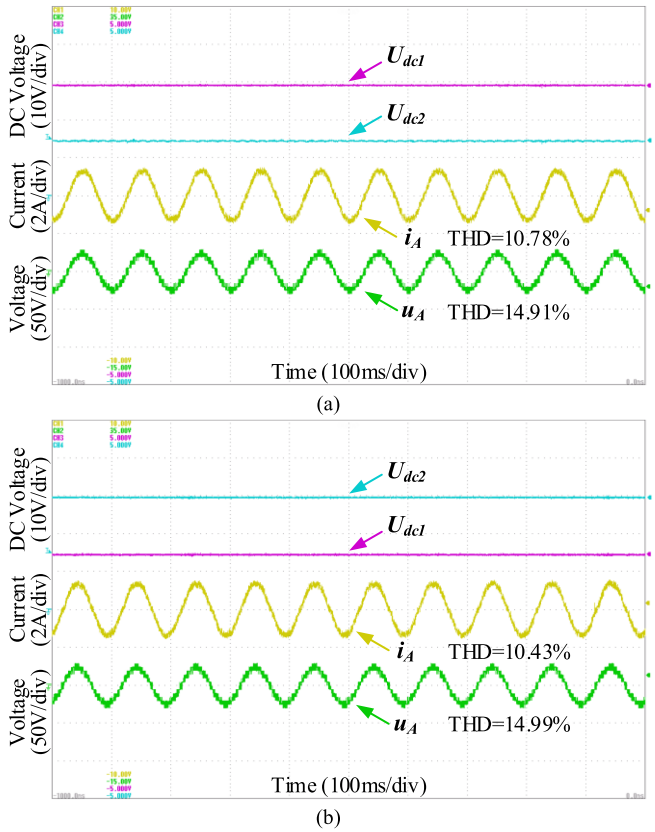

Fig. 10. Experimental waveforms when dual inverters act as the master inverter, respectively. (a) INV1 acts as the master inverter. (b) INV2 acts as the master inverter.

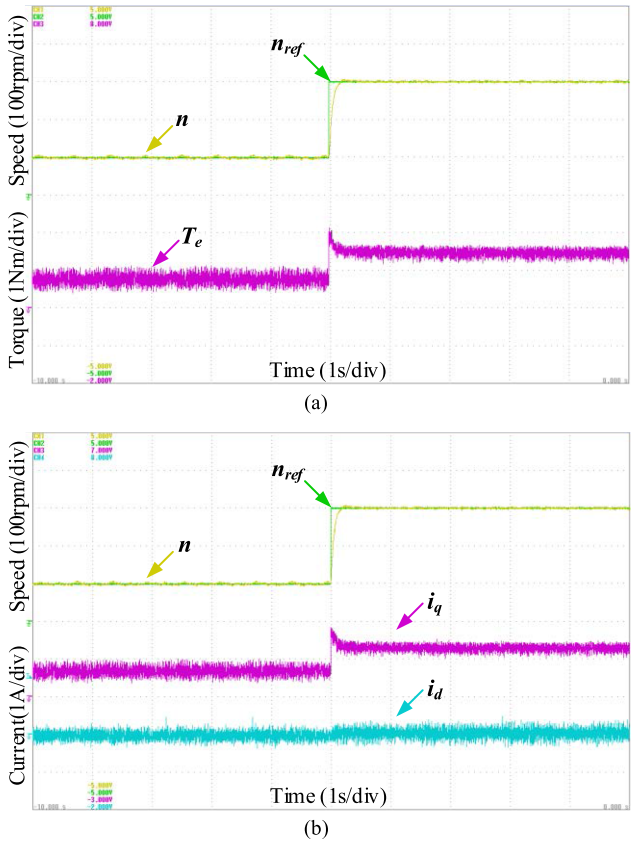

Fig. 11. Experimental waveforms with the speed step from 100 to 300 rpm. (a) Speed and output torque. (b) dq-axis currents.

currents and voltages in the two cases are 10.78%, 10.43% and 14.91%, 14.99%, respectively. The control performances of the proposed strategy in the two cases are identical, which can also prove the correctness of the proposed switching algorithm of the master inverter and the slave inverter.

Fig. 11 presents the dynamic performance of the proposed MPC strategy with the speed step from 100 to 300 rpm. In the experiment, the real motor speed tracks its suddenly changed reference value rapidly and accurately. The output torque changes as the reference speed mutate, and then it could converge to the new stable value quickly in Fig. 11(a). The q-axis current also goes through a transition to support the torque output, and the d-axis current remains stable during the entire dynamic process, as is shown in Fig. 11(b).

The dynamic experimental performance of the proposed MPC strategy with a load step at 300 rpm is shown in Fig. 12. During the experiment, the load torque is suddenly changed by adjusting the load resistance with a breaker. As is shown in Fig. 12, the motor speed experienced a small drop and then returns to its reference value quickly. The torque and q-axis current of the OW-PMSM could respond fast to the load change and stabilize to their new steady-state values. The d-axis current remains stable during the dynamic process.

The comparison of experimental phase-current THDs of the proposed MPC strategy with different dc-link voltage ratios under 300 rpm is shown in Fig. 13. For a fair comparison,

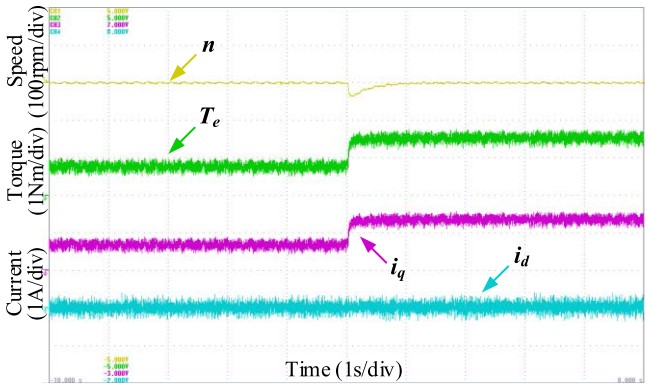

Fig. 12. Experimental waveforms with the load torque variation.

the sums of dc voltages from both sides are set equal in the experiments with different voltage ratios. As is seen in the diagram, the proposed MPC strategy for OW-PMSM can greatly reduce the current THD by generating multilevel voltage. It can be concluded from Fig. 13 that the power quality of the OW-PMSM drive is optimal when the voltage ratio is around 3:1 and 2:1, as expected. The high-order current harmonics are mainly produced by the inverters' switching actions. By utilizing the multilevel characteristics of the OW-PMSM drive with an unfixed voltage ratio of dc buses in the proposed MPC strategy,

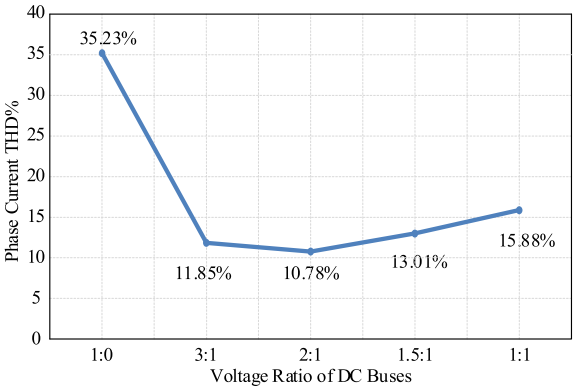

Fig. 13. Phase current THD of different DC voltage ratios.

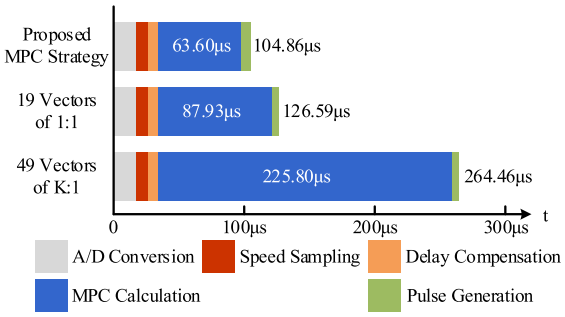

Fig. 14. Calculation times of different MPC strategies.

the high-order current harmonics can be greatly reduced. For some drive applications with higher requirements for power quality, electric reactors can be adopted between the motor and the inverters to further reduce the current harmonics.

To further prove the universal applicability and excellent power quality of the proposed strategy for different voltage ratios, the experimental THD comparison of the representative MPC strategies with different voltage ratios is shown in Table III. Strategy-I and Strategy-II in Table III are two typical MPC strategies of the OW-PMSM drive, respectively, designed for the voltage ratios of 1:1 and 2:1. It can be found that the two MPC strategies can operate with relatively low current harmonics at their respective matched voltage ratios, namely 16.36% of Strategy-I at the voltage ratio of 1:1 and 11.05% of Strategy-II at the voltage ratio of 2:1. However, they can hardly fully utilized the multilevel characteristics of OW-PMSM drive with unmatched voltage ratios to reduce the current harmonics. By comparison, the proposed MPC strategy can always operate with lower current harmonics under different voltage ratios, which proves that the proposed MPC strategy can fully utilize the multilevel characteristics of OW-PMSM drives with arbitrary voltage ratios to improve the power quality.

In order to evaluate the calculation workload occupied by the MPC calculation more intuitively, Fig. 14 illustrates the running time comparisons of different MPC strategies in the DSP controller. As can be seen from different MPC strategies in Fig. 14, the MPC parts account for a much longer execution time than the basic calculation parts, such as A/D conversion and speed sampling, which indirectly proves the necessity of reducing the number of the candidate vectors in MPC. In Fig. 14, the execution time of the basic calculation parts in different MPC strategies is almost identical. The MPC calculations in the 1:1 conventional MPC strategy with 19 candidate vectors and K:1 MPC strategy with 49 candidate vectors occupy the time of 87.93 and 225.80 μs, respectively. By comparison, the proposed MPC strategy with less than 15 candidate vectors only needs 63.60 μs with a significant reduction of computation burden, which proves the superiority of the proposed MPC strategy in the aspect of calculation burden reduction.

VI. Conclusion

This article proposed a universal MPC strategy for OW-PMSM drives with arbitrary dc-link voltage ratios. By choosing the vectors adjacent to the output vector of the last control cycle as the candidate vectors, the proposed control can reduce the number of the vectors to be calculated from 49 to less than 15. This greatly reduces the computational burden without sacrificing the output power quality. Besides, the proposed MPC strategy is applicable for any voltage ratio of the two separate dc buses by appointing the master inverter flexibly according to the voltage relationship of dc buses, which significantly improves the adaptability of the proposed strategy. Experiments are designed and implemented to verify the effectiveness and superiority of the proposed strategy.

References

[1] M. S. R. Saeed, W. Song, B. Yu, Z. Xie, and X. Feng, "Low-complexity deadbeat model predictive current control for open-winding PMSM drive with zero-sequence current suppression," *IEEE Trans. Transp. Electrific.*, vol. 7, no. 4, pp. 2671–2682, Dec. 2021.

[2] X. Yuan, S. Zhang, C. Zhang, M. Degano, G. Buticchi, and A. Galassini, "Improved finite-state model predictive current control with zero-sequence current suppression for OEW-SPMSM drives," *IEEE Trans. Power Electron.*, vol. 35, no. 5, pp. 4996–5006, May 2020.

[3] X. Wang, Z. Wang, M. He, Q. Zhou, X. Liu, and X. Meng, "Fault-tolerant control of dual three-phase PMSM drives with minimized copper loss," *IEEE Trans. Power Electron.*, vol. 36, no. 11, pp. 12938–12953, Nov. 2021.

[4] X. Wang, Z. Wang, Z. Xu, J. He, and W. Zhao, "Diagnosis and tolerance of common electrical faults in t-type three-level inverters fed dual three-phase PMSM Drives," *IEEE Trans. Power Electron.*, vol. 35, no. 2, pp. 1753–1769, Feb. 2020.

[5] W. Hu, H. Nian, and D. Sun, "Zero-sequence current suppression strategy with reduced switching frequency for open-end winding PMSM drives with common DC BUS," *IEEE Trans. Ind. Electron.*, vol. 66, no. 10, pp. 7613–7623, Oct. 2019.

[6] Y. Cheng, D. Sun, W. Chen, and H. Nian, "Model predictive current control for an open-winding PMSM system with a common DC bus in 3-D space," *IEEE Trans. Power Electron.*, vol. 35, no. 9, pp. 9597–9607, Sep. 2020.

[7] D. Sun, W. Chen, Y. Cheng, and H. Nian, "Improved direct torque control for open-winding PMSM system considering zero-sequence current suppression with low switching frequency," *IEEE Trans. Power Electron.*, vol. 36, no. 4, pp. 4440–4451, Apr. 2021.

[8] C. Sun, D. Sun, W. Chen, and H. Nian, "Improved model predictive control with new cost function for hybrid-inverter open-winding PMSM system based on energy storage model," *IEEE Trans. Power Electron.*, vol. 36, no. 9, pp. 10705–10715, Sep. 2021.

[9] J. E. Huber and J. W. Kolar, "Optimum number of cascaded cells for high-power medium-voltage AC–DC converters," *IEEE J. Emerg. Sel. Topics Power Electron.*, vol. 5, no. 1, pp. 213–232, Mar. 2017.

[10] J. Saha, N. B. Y. Gorla, and S. K. Panda, "Implementation of power balance control scheme for a cascaded matrix-based dual-active-bridge (CMB-DAB) MVAC-LVDC Converter," *IEEE Trans. Ind. Appl.*, vol. 58, no. 1, pp. 388–399, Jan./Feb. 2022.

[11] J. Pereda and J. Dixon, "Cascaded multilevel converters: Optimal asymmetries and floating capacitor control," *IEEE Trans. Ind. Electron.*, vol. 60, no. 11, pp. 4784–4793, Nov. 2013.
[12] Z. Huang, T. Yang, P. Giangrande, S. Chowdhury, M. Galea, and P. Wheeler, "An active modulation scheme to boost voltage utilization of the dual converter with a floating bridge," *IEEE Trans. Ind. Electron.*, vol. 66, no. 7, pp. 5623–5633, Jul. 2019.
[13] K. R. Sekhar and S. Srinivas, "Discontinuous decoupled PWMs for reduced current ripple in a dual two-level inverter fed open-end winding induction motor drive," *IEEE Trans. Power Electron.*, vol. 28, no. 5, pp. 2493–2502, May 2013.
[14] E. G. Shivakumar, K. Gopakumar, S. K. Sinha, A. Pittet, and V. T. Ranganathan, "Space vector PWM control of dual inverter fed open-end winding induction motor drive," in *Proc. 16th Annu. IEEE Appl. Power Electron. Conf. Expo.*, 2001, pp. 399–405.
[15] S. Lakhimsetty and V. T. Somasekhar, "An efficient predictive current control strategy for a four-level open-end winding induction motor drive," *IEEE Trans. Power Electron.*, vol. 35, no. 6, pp. 6198–6207, Jun. 2020.
[16] M. Wang, D. Sun, W. Ke, and H. Nian, "A universal lookup table-based direct torque control for OW-PMSM Drives," *IEEE Trans. Power Electron.*, vol. 36, no. 6, pp. 6188–6191, Jun. 2021.
[17] Z. Huang, T. Yang, P. Giangrande, S. Chowdhury, M. Galea, and P. Wheeler, "Enhanced performance of dual inverter with a floating capacitor for motor drive applications," *IEEE Trans. Power Electron.*, vol. 36, no. 6, pp. 6903–6916, Jun. 2021.
[18] M. Chen and D. Sun, "A unified space vector pulse width modulation for dual two-level inverter system," *IEEE Trans. Power Electron.*, vol. 32, no. 2, pp. 889–893, Feb. 2017.
[19] S. Vazquez, J. Rodriguez, M. Rivera, L. G. Franquelo, and M. Norambuena, "Model predictive control for power converters and drives: Advances and trends," *IEEE Trans. Ind. Electron.*, vol. 64, no. 2, pp. 935–947, Feb. 2017.
[20] Y. Zhang, Y. Bai, H. Yang, and B. Zhang, "Low switching frequency model predictive control of three-level inverter-fed IM drives with speed-sensorless and field-weakening operations," *IEEE Trans. Ind. Electron.*, vol. 66, no. 6, pp. 4262–4272, Jun. 2019.
[21] D. Zhou, Z. Quan, and Y. Li, "Hybrid model predictive control of ANPC converters with decoupled low-frequency and high-frequency cells," *IEEE Trans. Power Electron.*, vol. 35, no. 8, pp. 8569–8580, Aug. 2020.
[22] C. Sun, D. Sun, Z. Zheng, and H. Nian, "Simplified model predictive control for dual inverter-fed open-winding permanent magnet synchronous motor," *IEEE Trans. Energy Convers.*, vol. 33, no. 4, pp. 1846–1854, Dec. 2018.
[23] R. E. K. Meesala, V. P. K. Kunisetti, and V. K. Thippiripati, "Enhanced predictive torque control for open end winding induction motor drive without weighting factor assignment," *IEEE Trans. Power Electron.*, vol. 34, no. 1, pp. 503–513, Jan. 2019.
[24] N. S. P. Musunuru and S. Srirama, "Cascaded predictive control of a single power supply-driven four-level open-end winding induction motor drive without weighting factors," *IEEE J. Emerg. Sel. Topics Power Electron.*, vol. 9, no. 3, pp. 2858–2867, Jun. 2021.
[25] Y. Wei, Y. Wei, Y. Sun, H. Qi, and X. Guo, "Prediction horizons optimized nonlinear predictive control for permanent magnet synchronous motor position system," *IEEE Trans. Ind. Electron.*, vol. 67, no. 11, pp. 9153–9163, Nov. 2020.
[26] S. Dai, J. Wang, Z. Sun, and E. Chong, "Multiple current harmonics suppression for low-inductance PMSM drives with deadbeat predictive current control," *IEEE Trans. Ind. Electron.*, vol. 69, no. 10, pp. 9817–9826, Oct. 2022.
[27] K. M. R. Eswar, K. V. P. Kumar, and T. V. Kumar, "A Simplified predictive torque control scheme for open-end winding induction motor drive," *IEEE J. Emerg. Sel. Topics Power Electron.*, vol. 7, no. 2, pp. 1162–1172, Jun. 2019.

Yancheng Chen (Student Member, IEEE) received the B.S. degree in electrical engineering and automation from the Sichuan University, Chengdu, China, in 2020. He is currently working toward the M.S. degree in electrical engineering with the Sichuan University, Chengdu, China.

His research interests include the control of open-winding permanent magnet synchronous motors, and the model predictive control strategy.

Xueqing Wang (Member, IEEE) received the B.S. degree in electrical engineering from the Tianjin University of Science and Technology, Tianjin, China, in 2014, and the M.S. and Ph.D. degrees in electrical engineering from the Southeast University, Nanjing, China, in 2016 and 2020, respectively.

From 2018 to 2019, he was a joint Ph.D. with the McMaster Automotive Resource Centre, McMaster University, Hamilton, ON, Canada. He is currently an Associate Research Fellow with the College of Electrical Engineering, Sichuan University, Chengdu, China. His research interests include control of multiphase motor and open-winding motor, fault diagnosis and tolerant control of motor drive, and multilevel PWM strategy.

Xin Meng (Member, IEEE) received the B.S. degree from the University of Electronic Science and Technology of China, Chengdu, China, in 2014, and the Ph.D. degree from the Xi'an Jiaotong University, Xi'an, China, in 2019, both in electrical engineering.

He joined the Electrical Engineering School, Sichuan University, Chengdu, China, as a Faculty Member. His research interests include the control of parallel three-phase inverters for uninterrupted power supply and microgrid application, such as VSG control, droop control, and seamless transfer between grid-connected mode and islanding mode.

Mingzhi He (Member, IEEE) received the B.S. and M.S. degrees from the College of Electrical Engineering, Sichuan University, Chengdu, China, in 2002 and 2004, respectively, and the Ph.D. degree from the Southwest Jiaotong University, Chengdu, China, in 2008, all in electrical engineering.

He is currently a Professor with the College of Electrical Engineering, Sichuan University. His interest includes the control & topology of switching power supply, photovoltaic system, battery charger, and protection.

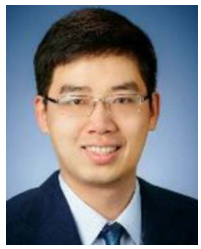

Dianxun Xiao (Member, IEEE) received the B.S. and M.S. degrees in electrical engineering from the Harbin Institute of Technology, Harbin, China, in 2016 and 2018, respectively, and the Ph.D. degree in electrical and computer engineering from the McMaster University, Hamilton, ON, Canada, in 2021.

He is currently an Assistant Professor with the Sustainable Energy and Environment Thrust, The Hong Kong University of Science and Technology (Guangzhou), Guangzhou, China. Before that, he was a Postdoctoral Research Fellow with the McMaster Automotive Resource Centre, McMaster University, Hamilton, ON, Canada, in 2021. His research interests include permanent magnet synchronous motor drives, switched reluctance motor drives, high-power converters, and battery management systems for transportation electrification applications.

Dr. Xiao is an Associate Editor for IEEE TRANSACTIONS ON TRANSPORTATION ELECTRIFICATION.

Zheng Wang (Senior Member, IEEE) received the B.Eng. and M.Eng. degrees from the Southeast University, Nanjing, China, in 2000 and 2003, respectively, and the Ph.D. degree from The University of Hong Kong, Hong Kong, in 2008, all in electrical engineering.

From 2008 to 2009, he was a Postdoctoral Fellow with the Ryerson University, Toronto, ON, Canada. He is currently a Full Professor with the School of Electrical Engineering, Southeast University. He has authored or coauthored more than 80 internationally refereed papers and 4 books. His research interests include electric drives, power electronics, and distributed generation.

Prof. Wang was the recipient of several academic awards including IEEE PES Chapter Outstanding Engineer Award, Best Paper Award of International Conference on Electrical Machines and Systems, Best Session Paper Award of IEEE Annual Meeting of Industrial Electronics, and Nanjing Outstanding Paper Award of Natural Science.